ORIGINAL ARTICLE

Notch1 Induces Defective Epithelial Surfactant Processing and Pulmonary Fibrosis

Roxana Wasnick¹, Martina Korfei¹, Katarzyna Piskulak¹, Ingrid Henneke^{1,2,3}, Jochen Wilhelm^{1,2,3}, Poornima Mahavadi^{1,2} Ruth Charlotte Dartsch¹, Daniel von der Beck¹, Miriam Koch^{1,4}, Irina Shalashova¹, Astrid Weiss¹, Oleksiy Klymenko¹, Ingolf Askevold⁵, Ludger Fink⁶, Heiko Witt⁷, Holger Hackstein⁸, Elie El Agha^{1,2,3}, Saverio Bellusci^{1,2,3}, Walter Klepetko⁹, Melanie Königshoff^{10,11}, Oliver Eickelberg¹¹, Ralph Theo Schermuly^{1,2,3}, Thomas Braun^{1,2,3,12}, Werner Seeger^{1,2,3,12}, Clemens Ruppert^{1,2,13*}, and Andreas Guenther^{1,2,3,4,13*}

¹University of Giessen and Marburg Lung Center (UGMLC), member of the German Center for Lung Research (DZL), 35392 Giessen, Germany; ²Excellence Cluster Cardiopulmonary Institute (CPI), 35392 Giessen, Germany; ³Institute for Lung Health (ILH), 35392 Giessen, Germany; ⁴Lung Clinic, Evangelisches Krankenhaus Mittelhessen, 35398 Giessen, Germany; ⁵Department of Surgery, Justus-Liebig-University Giessen, 35392 Giessen, Germany; ⁶Institut für Pathologie, Überregionale Gemeinschaftspraxis für Pathologie und Zytologie, 35578 Wetzlar, Germany; ⁷Pediatric Nutritional Medicine, Else-Kröner-Fresenius-Fresenius-Ceter for Nutritional Sciences, Technical University Munich, 85354 Freising, Germany; ⁸Department of Clinical Immunology and Transfusion Medicine, Justus-Liebig University Giessen, 35392 Giessen, Germany; ⁹Department of Thoracic Surgery, Vienna General Hospital, 1090 Vienna, Austria; ¹⁰Comprehensive Pneumology Center, Research Unit Lung Repair and Regeneration, Helmholtz Center Munich, Ludwig Maximilians University Munich, 81377 Munich, Germany; ¹¹Division of Pulmonary, Allergy, and Critical Care Medicine, University of Pittsburgh, Pittsburgh, PA 15261; ¹²Max-Planck-Institute for Heart and Lung Research, 61231 Bad Nauheim, Germany; and ¹³European IPF Registry/Biobank, 35392 Giessen, Germany

ORCID IDs: 0000-0003-1114-7799 (R.W.); 0000-0003-1946-9303 (D.v.d.B.); 0000-0001-9414-5128 (M. Königshoff); 0000-0001-7170-0360 (O.E.); 0000-0002-2187-0975 (A.G.).

Abstract

Rationale: Although type II alveolar epithelial cells (AEC2s) are chronically injured in idiopathic pulmonary fibrosis (IPF), they contribute to epithelial regeneration in IPF.

Objectives: We hypothesized that Notch signaling may contribute to AEC2 proliferation, dedifferentiation characterized by loss of surfactant processing machinery, and lung fibrosis in IPF.

Methods: We applied microarray analysis, kinome profiling, flow cytometry, immunofluorescence analysis, western blotting, quantitative PCR, and proliferation and surface activity analysis to study epithelial differentiation, proliferation, and matrix deposition *in vitro* (AEC2 lines, primary murine/human AEC2s), *ex vivo* (human IPF-derived precision-cut lung slices), and *in vivo* (bleomycin and pepstatin application, Notch1 [Notch receptor 1] intracellular domain overexpression).

Measurements and Main Results: We document here extensive SP-B and -C (surfactant protein-B and -C) processing defects in IPF AEC2s, due to loss of Napsin A, resulting in increased intra-alveolar surface tension and alveolar collapse and

induction of endoplasmic reticulum stress in AEC2s. *In vivo* pharmacological inhibition of Napsin A results in the development of AEC2 injury and overt lung fibrosis. We also demonstrate that Notch1 signaling is already activated early in IPF and determines AEC2 fate by inhibiting differentiation (reduced lamellar body compartment, reduced capacity to process hydrophobic SP) and by causing increased epithelial proliferation and development of lung fibrosis, putatively via altered JAK (Janus kinase)/Stat (signal transducer and activator of transcription) signaling in AEC2s. Conversely, inhibition of Notch signaling in IPF-derived precision-cut lung slices improved the surfactant processing capacity of AEC2s and reversed fibrosis.

Conclusions: Notch1 is a central regulator of AEC2 fate in IPF. It induces alveolar epithelial proliferation and loss of Napsin A and of surfactant proprotein processing, and it contributes to fibroproliferation.

Keywords: interstitial lung disease; diffuse parenchymal lung disease; lung surfactant; epithelial regeneration; idiopathic pulmonary fibrosis

(Received in original form May 26, 2022; accepted in final form August 29, 2022)

Supported by grants from the German Ministry of Science and Education (German Center for Lung Research, DA DPLD Funds), the European Commission (eurIPFnet, Seventh Framework Programme), the German Research Council (JLU CAREER, Excellency Cluster Cardio-Pulmonary System, KFO 309), and the Lung Fibrosis Foundation Waldhof-Elgershausen (Lung Fibrosis Stipend).

Am J Respir Crit Care Med Vol 207, Iss 3, pp 283–299, Feb 1, 2023 Copyright © 2023 by the American Thoracic Society Originally Published in Press as DOI: 10.1164/rccm.202105-1284OC on September 1, 2023 Internet address: www.atsiournals.org

^{*}These authors contributed equally to this work.

At a Glance Commentary

Scientific Knowledge on the Subject: Idiopathic pulmonary fibrosis (IPF) results from permanent type II alveolar epithelial cell (AEC2) injury. AEC2s represent an alveolar epithelial progenitor population, but their role in epithelial regeneration in IPF is unclear, as are the underlying signaling pathways.

What This Study Adds to the Field: We show that Notch1 (Notch receptor 1) signaling is increased in human IPF AEC2s and in experimental models of lung fibrosis and induces AEC2 proliferation in response to injury and development of lung fibrosis. In parallel, however, Notch1 signaling also causes defective processing of SP-B (surfactant protein B) and SP-C and, as a result, highly increased surface tension values at the alveolar air-water interface in vitro as well as in vivo. Accordingly, we show a clear increase in expiratory subpleural density, suggesting repetitive alveolar collapse, on high-resolution computed tomography from patients with IPF, but not patients with chronic obstructive pulmonary disease or control subjects. Finally, experimental blockade of Notch signaling in human IPF precision-cut lung slices cultured ex vivo for several days not only resulted in restoration of proper processing of SPs and of regular lipid synthesis and trafficking in AEC2s but also reduced markers of fibrosis on conventional trichrome staining and immunohistochemistry.

Idiopathic pulmonary fibrosis (IPF) is a progressive, devastating, and ultimately fatal

lung disease (1) involving a predisposing genetic background as well as exogenous second hits acting in and on the alveolar epithelium (2, 3).

In the normal human lung, type II alveolar epithelial cells (AEC2s) exist mostly in a highly differentiated state and play an essential role in producing, processing, and adequately secreting pulmonary surfactant, a lipoprotein mixture consisting largely of dipalmitoylated phosphatidylcholine, phosphatidylglycerol, and two extremely hydrophobic surfactant proteins, SP-B (surfactant protein B) and SP-C, both of which undergo extensive post-translational processing by proteases such as Napsin A in the lysosomal compartment (reviewed in Reference 4). Pulmonary surfactant covers the alveolar space and greatly lowers alveolar surface tension, making breathing possible at normal transpulmonary pressure gradients (5). In some familial cases of IPF, mutations in SP-C and SP-A have been disclosed, which may cause protein misfolding, protein aggregation, endoplasmic reticulum (ER) stress, and AEC2 injury (6) (reviewed in References 7 and 3). Although SP mutations are only rarely found in sporadic IPF, increased alveolar surface tension (8), possibly favoring alveolar collapse (9, 10), has been described previously, and ER stress is a common feature (11).

In the injured lung, the facultative progenitor role of AEC2s becomes evident and allows them to reenter the cell cycle and to ensure the homeostatic replacement and repair of the alveolar epithelium (type I alveolar epithelial cells [AEC1s], AEC2s) (12–14). In IPF AEC2s, developmental pathways such as sonic hedgehog (15), TGF- β (transforming growth factor- β) (16), and Wnt (17) are known to be reactivated, and Notch signaling has been suggested to be activated in response to injury (18, 19). Notch signaling relies on four receptors (NOTCH1 [Notch receptor 1] through NOTCH4) that bind to and are activated by

five ligands (DLL1 [Delta like canonical Notch ligand 1], DLL3, and DLL4 and Jagged1 [Jagged canonical Notch ligand 1] and Jagged2) (20). Upon ligand binding, the Notch receptor undergoes two cleavage events mediated by the γ -secretase and Presenilin complex. This results in the release of the Notch intracellular domain (NICD), which translocates into the nucleus and activates transcription of downstream target genes (20). In the lung, Hes1 (Hes family BHLH transcription factor 1) is the best characterized Notch1 downstream target gene (21). During embryogenesis and in postnatal airways, Notch signaling acts as a cell-fate regulator by modulating cell proliferation and differentiation (22, 23).

On the basis of a non-hypothesisdriven transcriptomic analysis of laserdissected septa demonstrating differentially regulated Notch signaling in still normalappearing areas in IPF, and in light of previous studies documenting the importance of Notch signaling in stem cell fate specification, we hypothesize that enhanced Notch signaling regulates AEC2 differentiation status, being characterized by impaired SP processing mediated by Napsin A and Cathepsin H. We also hypothesized that the resultant accumulation of proforms of hydrophobic SPs may cause additional ER stress to AEC2s. Indeed, in this study, we demonstrate widespread loss of SP processing with consecutive accumulation of SP intermediates and ER stress, as well as increased alveolar surface tension and collapse, most likely contributing to chronic epithelial injury in IPF. We show that Notch activation in murine AEC2s is sufficient to induce lung fibrosis and that Notch blockade restores the surfactant processing machinery, thus opening new avenues for therapeutic interventions in IPF.

Some of the results of these studies were previously published in preprint form (https://www.biorxiv.org/content/10.1101/580498v1).

Author Contributions: A.G., W.S., T.B., S.B., and O.E. designed and supervised the study. R.T.S. and A.W. designed and executed the kinome data. R.W., M. Korfei, C.R., R.C.D., K.P., P.M., M. Koch, H.H., M. Königshoff, E.E.A., O.K., and I.S. conducted experimental work. W.K. and I.A. prepared and provided human lung materials. L.F. provided pathological evaluation of human and animal data. Animal experiments were conducted primarily by I.H. J.W. undertook transcriptome analysis. H.W. conducted the sequencing work. D.v.d.B. performed human computed tomography analysis. A.G. and R.W. assembled the figures and wrote the manuscript.

Correspondence and requests for reprints should be addressed to Andreas Guenther, M.D., University of Giessen Medical School, Justus-Liebig-University Giessen, Klinikstrasse 36, 35392 Giessen, Germany. E-mail: andreas.guenther@innere.med.uni-giessen.de.

This article has a related editorial.

The article has an online supplement, which is accessible from this issue's table of contents at www.atsjournals.org.

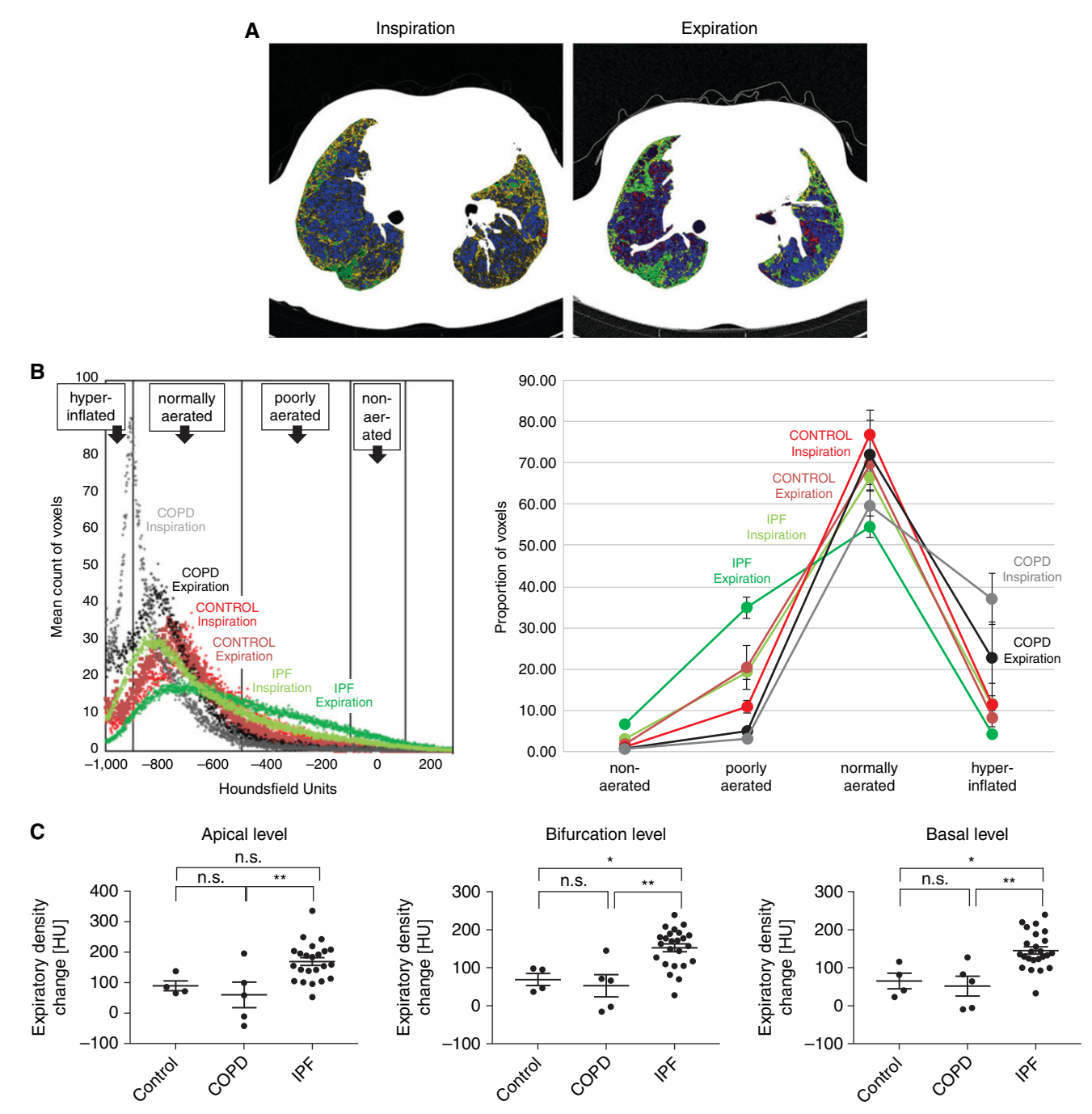


Figure 1. Expiratory alveolar collapse in patients with idiopathic pulmonary fibrosis (IPF). (A) Representative high-resolution computed tomography (HRCT) from one patient with IPF during inspiration and expiration. Voxels were color coded according to their density in Hounsfield units (HU; hyperinflated, -1,000 to -901 HU [red]; normally aerated, -900 to -501 HU [blue]; poorly aerated, -500 to -101 HU [yellow]; nonaerated, -100 to 100 HU [green]). Note the preferentially subpleural increase in green areas in expiration, indicating alveolar collapse. (B) Density distribution in HU in basal horizontal HRCT sections from pooled IPF (n=24), chronic obstructive pulmonary disease (COPD) (n=5), and control (n=4) groups during inspiration and expiration (left) and categorical distribution of voxels into nonaerated, poorly aerated, and normally aerated as well as hyperinflated lung areas (right). Individual sections were hand selected, transferred, and analyzed for HU distribution. All data from all patients per group were pooled and are given as mean densitogram for the three patient categories and inspiration versus expiration (left). The right panel shows the percentage of voxels per each density group for the same patient groups in inspiration and expiration. For the nonaerated tissue, differences reached significance for IPF versus control (P=0.027 at expiration; P=0.057 at inspiration), for IPF versus COPD (P<0.001 at expiration; P=0.006 at inspiration), but not for control versus COPD. In the poorly aerated tissue, differences reached significance for IPF versus control (P=0.034 at expiration; P=0.032 at inspiration), for IPF versus COPD (P<0.001 at expiration; P=0.006 at inspiration; P=0.006 at inspiration; P=0.006 at inspiration, and apical levels in expiration versus inspiration in the same patients as outlined in B. Data are presented as mean \pm SEM. *P<0.05 and *P<0.01 n.s. = not significant by ANOVA.

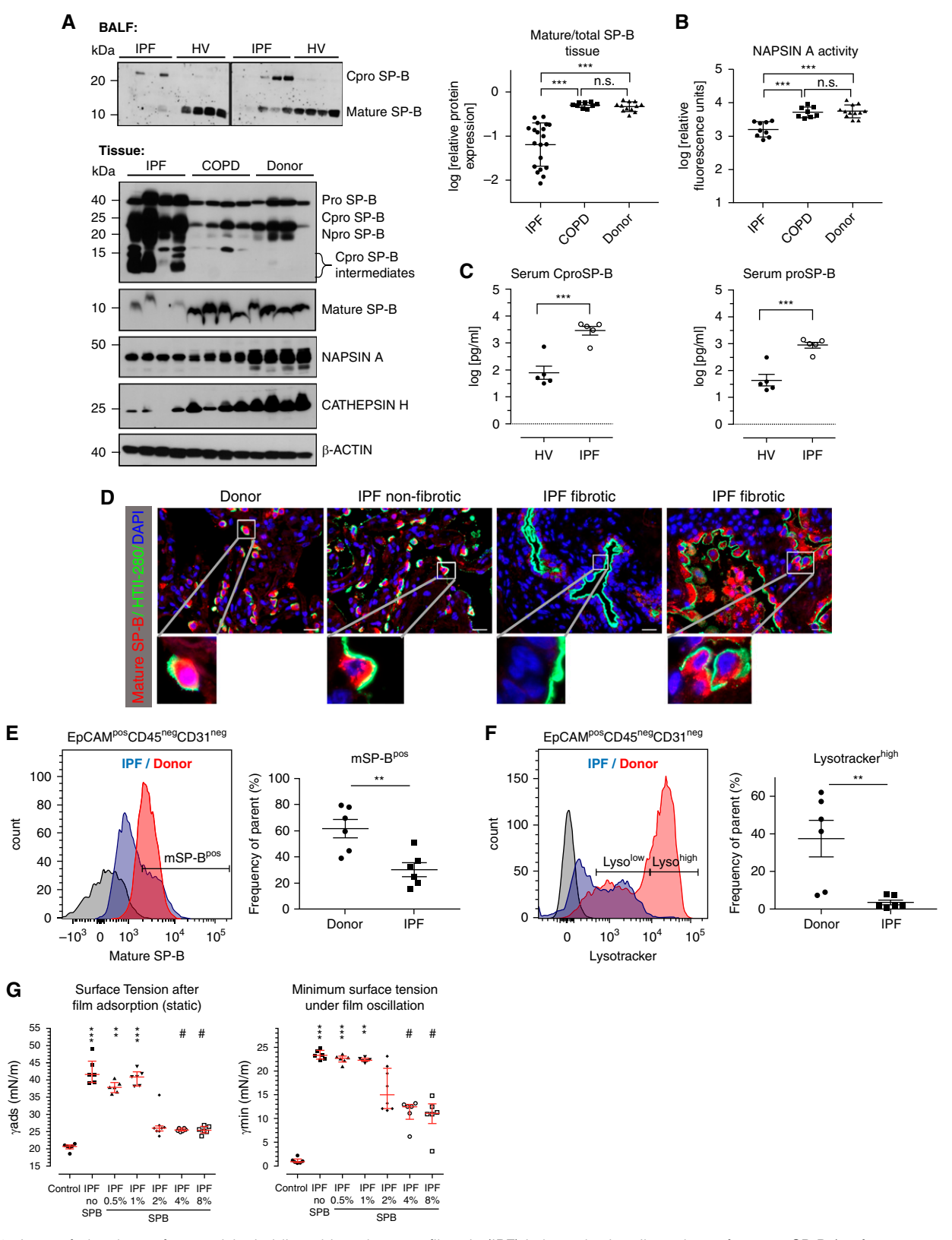


Figure 2. Loss of alveolar surface activity in idiopathic pulmonary fibrosis (IPF) is based primarily on loss of mature SP-B (surfactant protein B). (A) Upper panels: western blot analysis for mature SP-B (mSP-B) in the BALF of patients with IPF (n = 10) and healthy volunteers (n = 8). Lower panels: western blot analysis for mSP-B, Napsin A, and Cathepsin H in the peripheral lung tissue of subjects with IPF (n = 20), subjects with chronic obstructive pulmonary disease (COPD) (n = 9), and human donors (n = 12). The ratio of mSP-B to total SP-B in the peripheral lung tissue

Methods

An extensive and complete description of all applied methods is provided in the online supplement. In the following we provide essential information on patients and novel methods.

Patient and Control Groups

The study protocol was approved by the Ethics Committee of the Justus-Liebig-University School of Medicine (31/93, 29/01, and 111/08; University of Giessen and Marburg Lung Center Giessen Biobank and European IPF Registry/Biobank), and informed consent was obtained in writing from each subject (see Table E1 in the online supplement). Explanted lungs and human donor lung lobes or pieces resected for size incompatibilities were obtained during lung transplantation. Additional IPF lung tissue samples were obtained during diagnostic video-assisted thoracic surgery. BAL fluid (BALF) and blood were collected from patients with IPF and healthy volunteers. All IPF diagnoses were made according to the American Thoracic Society/European Respiratory Society consensus criteria (1), and a usual interstitial pneumonia pattern was consistently shown.

Precision-Cut Lung Slice Generation and Culture

One segment of each explanted human IPF lung was filled with 1.5% low-melt agarose at 37° C and allowed to cool on ice for 30 minutes. Blocks of tissue of $\sim 3 \times 3 \times 4$ cm (depth \times width \times height) were sectioned (500 μ m) using a vibrating-blade microtome and cultured for 4 days in Dulbecco's modified Eagle's medium/F12 (10% human serum, 1% penicillin/streptomycin, N-[N-(3,5-difluorophenacetyl-L-alanyl)]-S-phenylglycine

t-butyl ester [DAPT] [$10-50~\mu M$]) or DMSO (1:1,000). Medium was changed daily. Precision-cut lung slices (PCLSs) were then 1) fixed with 4% paraformaldehyde for 20 minutes, embedded in paraffin, and sectioned at 3 μm ; 2) homogenized in the lysis buffer used for western blot analysis; or 3) dissociated using dispase (Corning; 1:10 dilution) for 45 minutes at 37°C and processed for flow cytometry.

Results

Expiratory Alveolar Collapse in Patients with IPF

Alveolar collapse during expiration was analyzed on high-resolution computed tomography scans obtained during inspiration and end-expiration from patients with IPF, patients with chronic obstructive pulmonary disease (COPD), and control subjects. We observed an increase in subpleural density during expiration in individual IPF cases, corresponding to an increase in nonaerated lung areas (Figure 1A). We then assessed the density distribution (in Hounsfield units) in the entire basal layers of the pooled IPF, COPD, and control groups in inspiration and expiration. As evident from Figure 1B, patients with IPF showed a higher percentage of lung areas that were poorly aerated or nonaerated (24, 25) at the end of expiration, and this was similarly seen when analyzing the data using a categorical approach (Figure 1B, right panel). Finally, when analyzing the total subpleural space of hand-segmented, transversal computed tomography layers from the basal, bifurcation, and apical levels, patients with IPF showed a significantly higher increase in subpleural density at the end of expiration

not only at the basal level, where the disease is usually more prominent, but also in the most apical levels, where fibrotic changes are usually less apparent (26) (Figure 1C).

Loss of Alveolar Surface Activity in IPF Is a Result of Defective Processing of Hydrophobic SP-B and SP-C

Alveolar collapse may be caused by increased alveolar surface tension (8). We analyzed pulmonary surfactant composition in the BALF of healthy volunteers and subjects with IPF and in lung homogenates from agematched organ donors, patients with COPD, and those with IPF undergoing lung transplantation (see Table E1). In IPF BALF, a prominent loss of mature SP-B (mSP-B; Figure 2A) and mature SP-C (mSP-C; see Figure E1A) and appearance of the 23-kD C-terminal proSP-B intermediate (Figure 2A) and the 21-kD proSP-C (see Figure E1A) was encountered. In IPF homogenates, a comparable loss of mSP-B (Figure 2A; see quantification in Figure E1B) and mSP-C (see Figure E1A) was evident and was accompanied by pronounced tissue accumulation of the 42-kD SP-B precursor, the 23-kD C-terminal and 20-kD N-terminal proSP-B peptides, and smaller C-terminal processing intermediates of SP-B in the range of 12-16 kD (Figure 2A; see Figure E1B), as well as an elevation of proSP-B and C-terminal proSP-B intermediate in IPF sera (Figure 2C). As a result, the ratio of mSP-B to total SP-B was found to be profoundly decreased in IPF lung tissues (Figure 2B). In parallel, the peptidases Napsin A and Cathepsin H, which under normal conditions are responsible for processing of SP-B and SP-C proproteins in the lysosomal compartment, were profoundly reduced in protein concentration and activity

Figure 2. (*Continued*). is shown in the adjacent graph. Data are presented as mean \pm SEM. (*B*) NAPSIN A activity in peripheral lung tissue from patients with IPF (n=9) and COPD (n=9) and from human donors (n=12), as determined with a fluorogenic substrate. Data are presented as mean \pm SEM. ***P<0.001 by Student's t test. (*C*) Serum concentrations of proSP-B and CproSP-B in patients with IPF (n=5) and healthy control subjects (n=5). Data are presented as mean \pm SEM. ***P<0.001 by Student's t test. (*D*) Representative immunofluorescence staining for HTII-280 (green) and mSP-B (red) in human donor and IPF lung tissue (n=9 donors, n=10 patients with IPF). Scale bars, 20 μm. (E and F) Representative histograms of flow cytometry analysis of mSP-B (E) and LysoTracker incorporation (F) in the epithelial compartment of the lung, defined as the EpCAM^{pos} CD45^{neg} CD31^{neg}. The proportions of mSP-B^{high} and LysoTracker^{high} are quantified in the adjacent graphs (n=6 donors, n=6 patients with IPF). Data presented as mean \pm SEM. **P<0.01 by Student's t test. (G) Analysis of surface tension (γ) in large surfactant aggregate pools from healthy volunteers (n=5) and patients with IPF (n=15) at the end of 12 seconds of film adsorption (static, left graph) and under dynamic film oscillation in the pulsating bubble surfactometer after mSP-B supplementation (n=5 healthy volunteers and n=15 patients with IPF; percentages are relative amounts of mSP-B in relation to phospholipid, w/w). Given is the minimum surface tension after 5-minute film oscillation at a rate of 20 times per minute (right graph). Data are presented as mean \pm SEM. **P<0.01 and ***P<0.001 compared with control; *P<0.05 compared with IPF without SP-B (by ANOVA). BALF = BAL fluid; CD = cluster of differentiation; CproSP-B = C-terminal proSP-B intermediate; EpCAM = epithelial cell adhesion molecule; HV = healthy volunteer; Lyso = LysoTracker; n.s. = not significant.

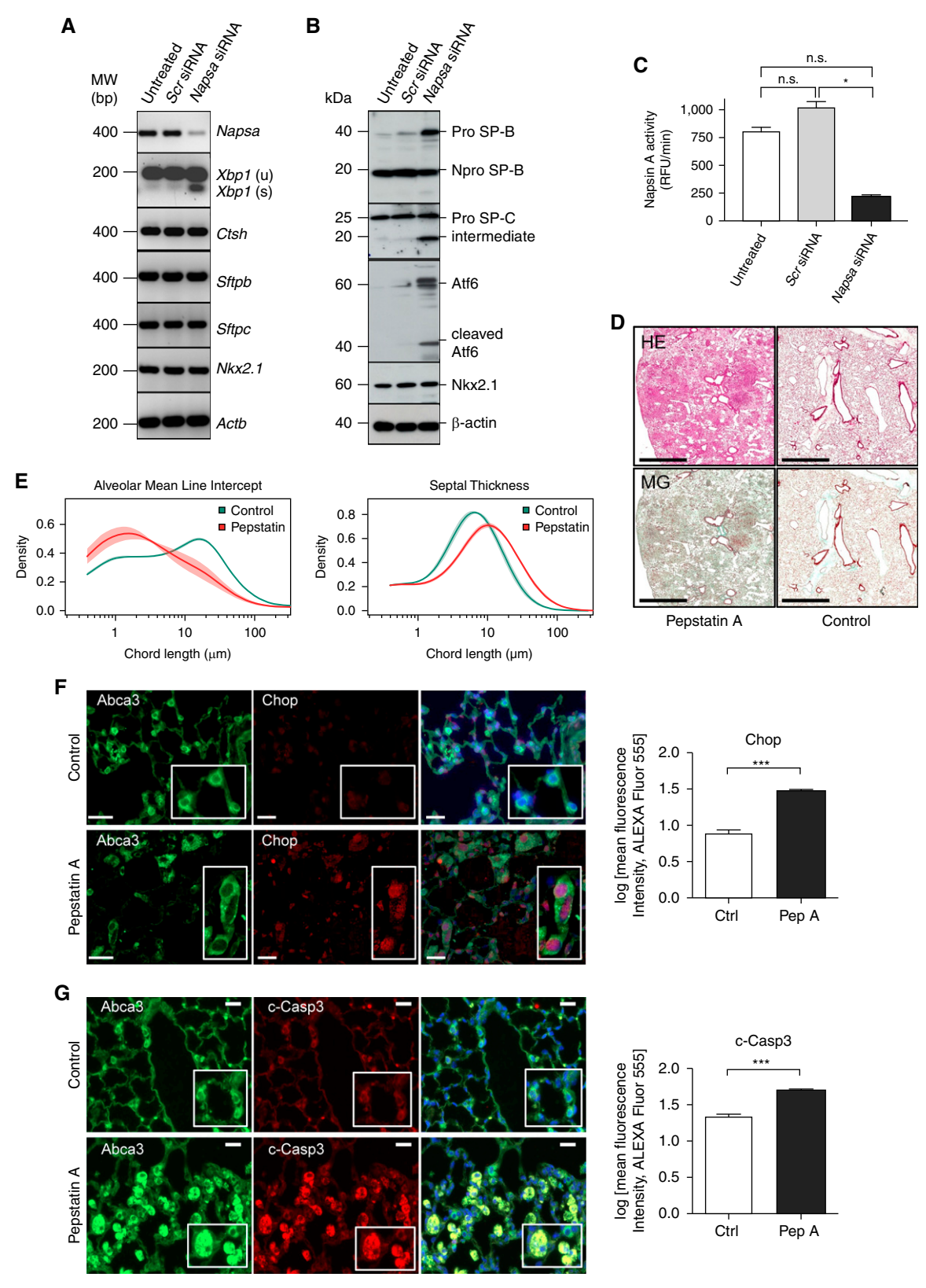


Figure 3. Inhibition of SP-B (surfactant protein B) processing recapitulates all features of lung fibrosis. (*A*) RT-PCR analysis of *Napsa* (Napsin A aspartic peptidase) and spliced and unspliced *Xbp1*, *Ctsh*, *Sftpb*, *Sftpc*, and *Nkx2.1* transcripts in MLE12 cells 2 days after *Napsa* siRNA transfection. (*B*) Western blot analysis of proSP-B, proSP-C, Atf6 (an endoplasmic reticulum stress marker), and Nkx2.1 in *Napsa* siRNA–transfected MLE12 cells 6 days after transfection. Untreated cells and cells transfected with Scr siRNA served as the controls.

(Figures 2A and 2B; see Figure E1B). Tissue stores of the phospholipids phosphatidylcholine and phosphatidylglycerol were also significantly reduced in IPF compared with (age-matched) subjects with COPD and donors (see Figure E1E). Genotyping of SP-B, SP-C, and NAPSIN A did not reveal any mutations in IPF (see Table E2), confirming that post-translational processing was altered in patients with IPF.

Using immunohistochemistry, mSP-C (see Figure E1C) and mSP-B (Figure 2D; see Figure E1D) were easily detected and colocalized with the AEC2 markers HTII-280 and ABCA3 (ATP-binding cassette subfamily A member 3) in donor tissues and in normal-appearing areas of IPF lungs. However, in fibrotic areas of IPF lungs, expression of mSP-B and mSP-C was heterogeneous, with areas of adjacent, hyperplastic HTII-280^{pos} AEC2s expressing comparable concentrations of mSP-B mixed with areas of HTII-280pos AEC2s devoid of mSP-B or mSP-C (Figure 2D; see Figures E1C and E1D). Of note, analysis of publicly available human single-cell RNA (scRNA) data available through the IPF Cell Atlas (http://www.ipfcellatlas.com) (27) and of our previously published AEC2-population transcriptomic data (28) revealed that neither SFTPC (surfactant protein C) nor SFTPB (surfactant protein B) is differentially expressed in AEC2s of patients with IPF compared with donors (see Figures E2A and E2B). However, a small transitional population of aberrant basaloid cells expressing low amounts of SFTPC and SFTPB was identified (see Figures E2A and E2B). Immunofluorescence detection of proSP-B and proSP-C in donor and IPF lung tissues also showed rather elevated expression of the two proforms of hydrophobic SP in fibrotic IPF areas compared with donor lungs (see Figure E2C). This points to surfactant processing

downregulation and not decreased protein production as a regulatory mechanism in IPF.

To further assess the surfactant compartment at the single-cell level, we determined using flow cytometry the amount of intracellular mSP-B and lamellar bodies (LysoTracker (Thermofisher) uptake [29]) of AEC2s in the EpCAM (epithelial cell adhesion molecule)pos CD45 (cluster of differentiation 45)^{neg} CD31^{neg} live population (Figures 2E and 2F; see Figure E3). We observed a striking decrease in the number and mean fluorescence intensity of mSP-B-positive and LysoTracker-positive cells. Analysis of IPF surgical biopsies obtained at the time of diagnosis revealed similar defects regarding processing of SP-B and -C (see Figure E1F), thus excluding a late-stage phenomenon.

Bleomycin treatment of mice caused similar changes in the hydrophobic SP processing machinery as observed in IPF, as evident from the loss of mSP-B and mSP-C in BALF (Figures 5F and 5G; see Figure E7A) and tissue (Figure 5H; see Figure E7B) and the prominent increase in proforms of SP-B (Figure 5H; see Figure E7B) seen at Day 7 and having a peak at Day 14 after bleomycin. Similar to human IPF lungs, a downregulation of the aspartyl protease Napsin A was found on mRNA and protein concentrations in response to bleomycin exposure, peaking at Day 14, which seemed to underlie these extensive changes in SP processing (Figures 5I and 5J). Reanalysis of a murine scRNA sequencing data set generated various time points after bleomycin exposure (30) revealed that neither SFTPC nor SFTPB is differentially expressed in mouse AEC2s after bleomycin injury and that a subpopulation of AEC2s called activated AEC2s was present at early time points after bleomycin injury (see Figure E7C). This adds

further evidence to the concept that impaired surfactant processing, rather than an overall reduction in SP expression, is responsible for the observed loss of mature SP in AEC2s in response to injury. Further down the differentiation path, an AEC2-to-AEC1 transitional population termed K8 (keratin 8)⁺ alveolar differentiation intermediate expressing low concentrations of SFTPC and SFTPB was also identified (*see* Figure E7C).

Pooled large surfactant aggregates from IPF BALF reconfirmed (8) an extensive loss of surface activity in IPF and supplementation of IPF large surfactant aggregates with mature bovine SP-B (0.5–8% w/w) alone was sufficient to greatly improve surface activity at a physiological relative SP-B concentration of 2–4% (5) (Figure 2G). Taken together these results demonstrate defective processing of SP-B at early disease stages, ultimately resulting in increased surface tension and cyclic alveolar collapse.

Inhibition of SP-B Processing Recapitulates All Features of Lung Fibrosis

We next investigated the cellular consequences of intracellular accumulation of proSP-B, as encountered in IPF. siRNA-mediated downregulation of *napsin A* in murine lung epithelial 12 (MLE12) cells resulted in accumulation of 42-kD proSP-B and proSP-C intermediates and induction of ER stress, as indicated by XBP-1 (X-box binding protein 1) splicing and increased ATF6 (activating transcription factor 6) expression and cleavage (Figures 3A–3C).

Daily transbronchial administration of the Napsin A inhibitor pepstatin A into the lungs of C57BL/6N mice for 28 days (n = 4 per group) resulted in a marked increase in proSP-B but not proSP-C (see Figure E4). Pepstatin A treatment resulted in reduced

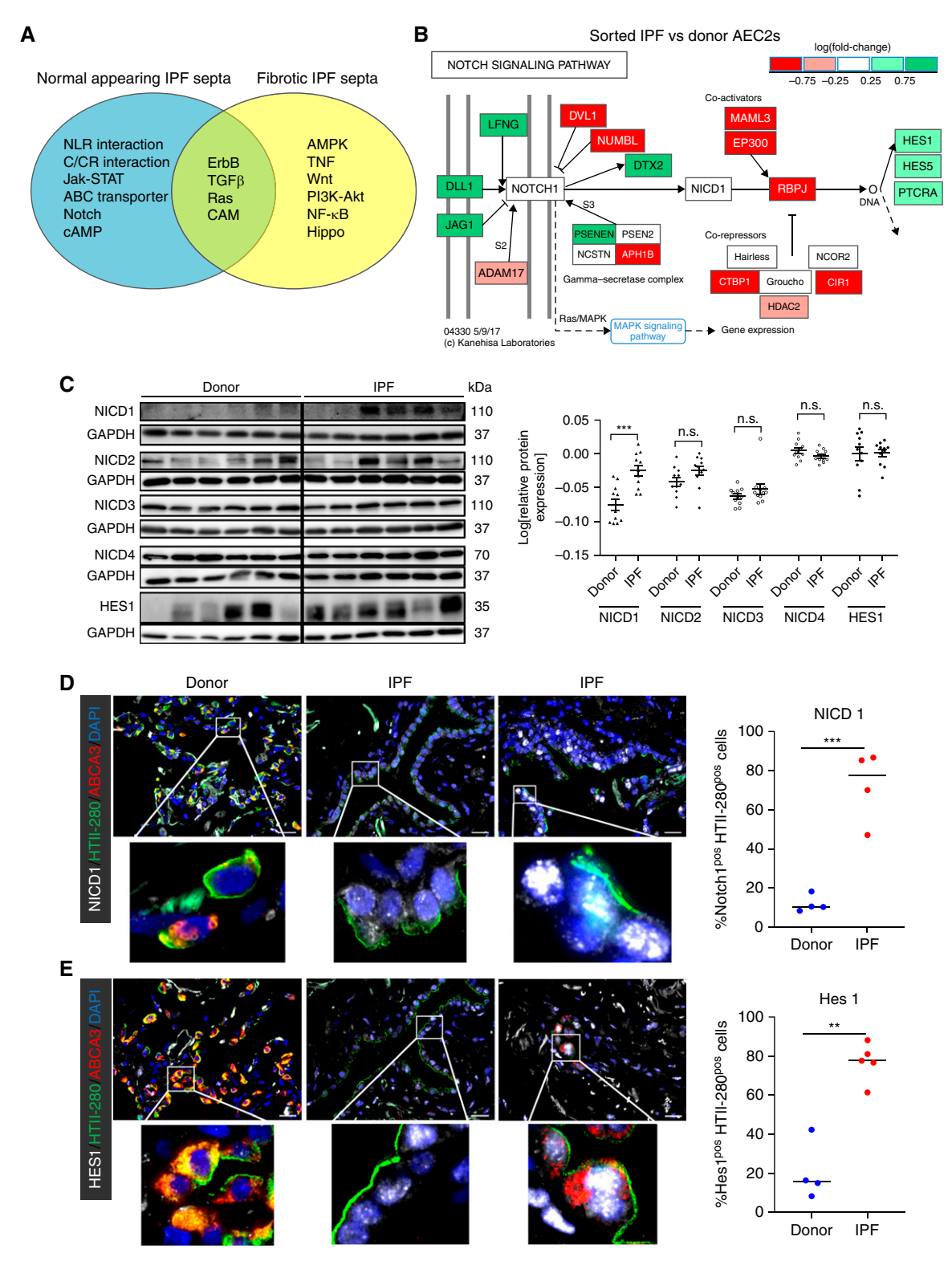


Figure 4. Notch1 (Notch receptor 1) signaling is upregulated in type II alveolar epithelial cells (AEC2s) from patients with idiopathic pulmonary fibrosis (IPF). (A) Venn diagram displaying signaling pathways differentially regulated in normal-appearing (blue) and fibrotic (yellow) septa from patients with IPF (n= 10) compared with donor septa (n= 7), with commonly regulated pathways in the intersection. (B) Diagram showing a reanalysis of atranscriptomic data set of sorted IPF (n= 6) versus donor (n= 8) AEC2s regarding regulation of the Notch pathway in these cells (B) (B) Western blot analysis and densitometric quantification of Notch receptor intracellular domains (NOTCH1-4) and HES1 (Hes family BHLH transcription factor 1) expression in donor (B= 11) and IPF (B= 11) lung homogenates. GAPDH served as loading control. Data are

survival (pepstatin A, 70%; control, 100%) and significant loss of pulmonary compliance $(4.9\pm0.5~{\rm vs.}~7.3\pm0.6~{\rm ml/kg}$ body weight; P=0.0002). Patchy and peribronchial lung fibrosis developed (Figure 3D), together with increased tissue content and loss of airspace (Figure 3E). In parallel, in AEC2s of pepstatin-treated mice, induction of Chop (C/EBP homologous protein), alternative splicing of Xbp-1, and increased cleavage of Caspase 3 (see Figures E4C and E4D; Figures 3F and 3G) suggested a corresponding induction of ER stress and apoptosis.

Reactivation of Notch Signaling in IPF

Transcriptome analysis was performed on laser-microdissected and captured normalappearing, as well as fibrotic, IPF septa, which were compared with donor lung septa. Notch signaling was found to be differentially regulated in normal-appearing septa of the fibrotic lung (Figure 4A; see Table E3) still populated by bona fide AEC2s. This was underscored by a reanalysis of a published transcriptomic data set of sorted AEC2s (CD45^{neg} CD31^{neg} EpCAM^{pos} LysoTracker^{pos} cells) from n = 8donors and n = 6 IPF lungs (28), showing differential regulation of Notch signaling. Here, upregulated genes were involved mostly in Notch activation, while many of the pathway inhibitors were downregulated, resulting in an upregulation of the downstream target genes HES1, HES5, and PTCRA (pre T cell antigen receptor alpha) (Figure 4B; see Figure E5A). In line with these data, analysis of the NICD and Notch ligand expression showed significantly increased concentrations of NICD1 (Figure 4C; see Figure E5B) and DLL1 (see Figures E5B, E5C, and E5E) at the protein but not mRNA level; all other receptors and ligands were unchanged

(Figure 4C; see Figures E5B, E5D, and E5E). Immunofluorescence showed significantly increased nuclear expression of NICD1 and Hes1 in ABCA3- or HTII-280-expressing AEC2s in IPF lungs and, to a certain extent, also in other cell types (e.g., myofibroblasts; Figures 4D and 4E). In donor lungs, NICD1 was found in the nuclei of the bronchial epithelium and rarely and at much lower concentrations in AEC2s (Figure 4D and data not shown). DLL1 staining was predominantly found in IPF AEC2s (see Figure E5C). Finally, colocalization of the proliferation marker phospho-HistoneH3 with Hes1 indicated that some AEC2s undergoing active Notch signaling are also proliferative (see Figure E5F).

Notch1 Signaling Activation in Bleomycin-induced Fibrosis

Accordingly, we could not detect meaningful changes of Notch receptors and ligands in the bleomycin lung fibrosis model at the mRNA level (Figures 5A and 5B), but we did observe upregulation of NICD1 and Hes1 proteins in lung homogenates during the proliferative (Day 14) and fibrotic (Day 21) phases (Figure 5C). At Day 14, AEC2s near fibrotic regions expressed high concentrations of Notch1 and Hes1, contrasting their exclusive expression in the bronchial epithelium of control lungs (Figure 5D; see Figure E6A). An increase in Hes1 and nuclearization of NICD1 were also observed in AEC2 of pepstatin A-treated mice (see Figure E4E), suggesting that activation of Notch represents a more common feature of lung fibrosis. Finally, bleomycin treatment of PCLSs derived from one human donor lung for 48 hours led to a significant increase in nuclearization of NICD1 in AEC2s, suggesting that Notch activation is an

early event in the repair after injury (*see* Figures E6B and E6C).

Impact of Notch Signaling on Alveolar Epithelial Cell Proliferation *In Vitro*

Time-dependent microarray analysis of NICD1-overexpressing MLE12 cells identified a large number of differentially regulated cell cycle genes (see Figure E8A). Interestingly, 5 of the 10 pathways identified here (see Table E4) were also differentially regulated in IPF septa (CAMs, Jak [Janus kinase]-STAT [signal transducer and activator of transcription], C/CR interaction, ErbB, and TGF-β; Figure 4A), suggesting that Notch signaling is upstream of these pathways. Moreover, overexpression of NICD1 in MLE12 cells significantly increased their proliferation (see Figure E8B), whereas inhibition of Notch signaling by either siRNA-mediated downregulation of POFUT1 (protein O-fucosyltransferase 1) or DAPT treatment resulted in a significant suppression of proliferation in MLE12 cells (see Figures E8C and E8D). Isolated primary AEC2s from bleomycin-treated mice at Day 14 showed increased proliferation (see Figures E8E and E8F) in parallel with increased NICD1 expression (see Figure E8E). Notch inhibition by the γ-secretase inhibitor DAPT decreased their proliferation (see Figure E8G).

AEC2-Specific NICD1 Overexpression In Vivo Leads to Lung Fibrosis

To study the consequences of Notch1 activation in AEC2 fate, we used doxycycline (Dox)-inducible, AEC2-specific NICD1-IRES (internal ribosomal entry site)-nEGFP (nuclear-localized enhanced green fluorescent protein) overexpressing transgenic mice (termed NICD1 mice) (31). Transgene induction was variable, leading to

Figure 4. (Continued). presented as mean \pm SEM of log-transformed densitometric values. ***P<0.001 by unpaired Student's t test. (D and E) Immunofluorescence localization of HTII-280 (green), ABCA3 (red), NICD1 (Notch intracellular domain 1) (white in D), HES1 (white in E), in representative sections of donor (n=4) and IPF (n=4 for NICD1 and n=5 for Hes1) tissue samples. DAPI represents the nuclear counterstain. Scale bars, 20 μm. Quantification of the NICD1- and Hes1-expressing cells is shown in the adjacent graph. ***P<0.01 and ***P<0.001. ABC = ATP-binding cassette; ABCA3 = ATP-binding cassette subfamily A member 3; ADAM17 = ADAM metallopeptidase domain 17; AMPK = AMP-activated protein kinase; APH1B = Aph-1 homolog B, gamma-secretase subunit; CIR1 = corepressor interacting with RBPJ, CIR1; CTBP1 = C-terminal binding protein 1; DLL1 = Delta like canonical Notch ligand 1; DTX2 = Deltex E3 ubiquitin ligase 2; DVL1 = Dishevelled segment polarity protein 1; EP300 = E1A binding protein P300; HDAC2 = histone deacetylase 2; JAG1 = Jagged canonical Notch ligand 1; Jak = Janus kinase; LFNG = LFNG O-fucosylpeptide 3-beta-N-acetylglucosaminyltransferase; MAML3 = Mastermind like transcriptional coactivator 3; MAPK = mitogen-activated protein kinase; NCOR2 = nuclear receptor corepressor 2; NCSTN = nicastrin; NF-κB = nuclear factor-κB; NLR = nucleotide-binding domain, leucine-rich repeat containing; n.s. = not significant; NUMBL = NUMB like endocytic adaptor protein; P1SK = phosphatidylinositol-3-kinase; PSEN2 = presenilin 2; PSENEN = presenilin enhancer, gamma-secretase subunit; PTCRA = pre T cell antigen receptor alpha; RBPJ = recombination signal binding protein for immunoglobulin kappa J region; STAT = signal transducer and activator of transcription; TGFβ = transforming growth factor-β; TNF = tumor necrosis factor.

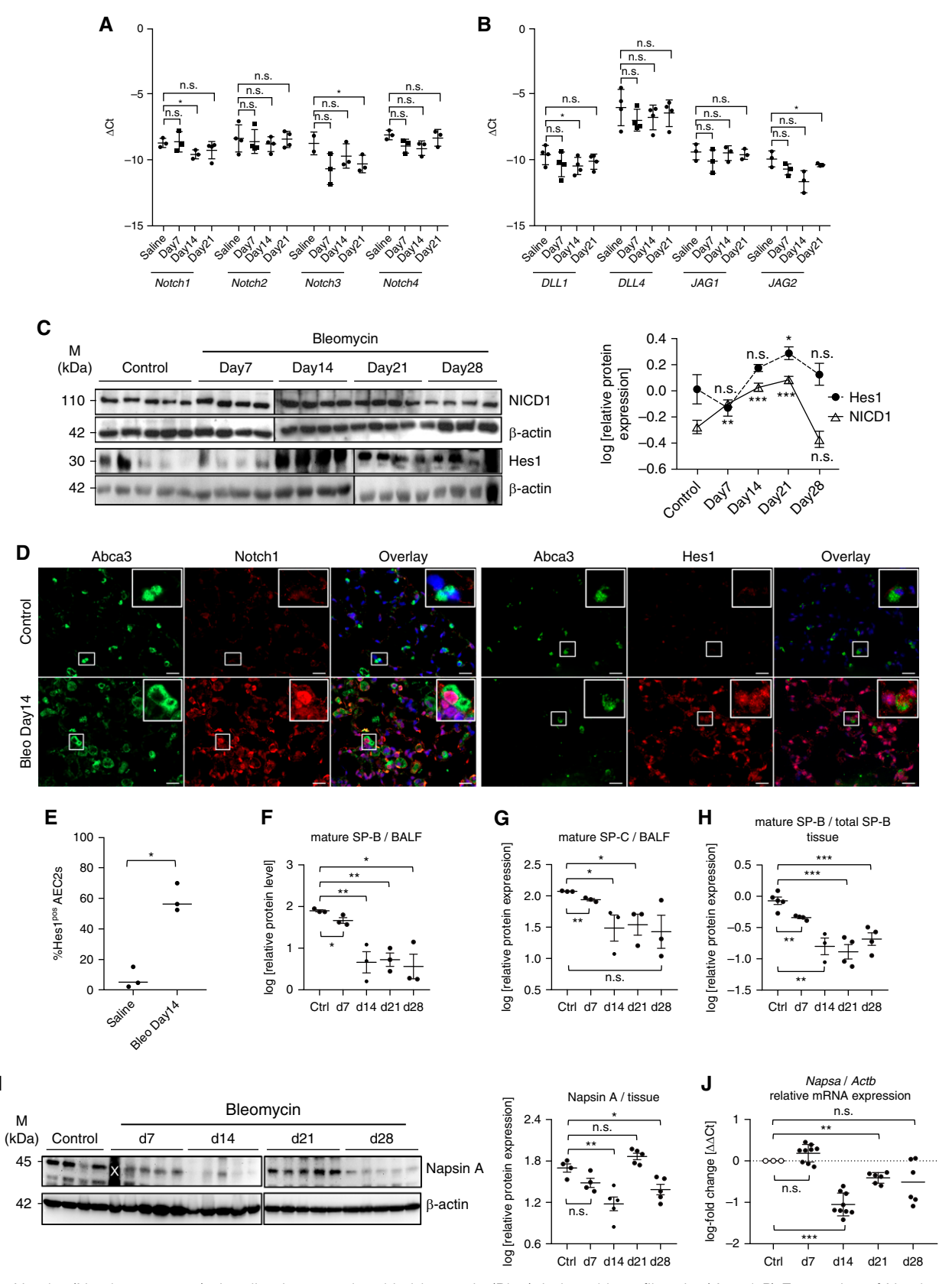


Figure 5. Notch1 (Notch receptor 1) signaling is upregulated in bleomycin (Bleo)-induced lung fibrosis. (*A* and *B*) Expression of Notch receptors 1–4 (*A*) and ligand (Dll1 [Delta like canonical Notch ligand 1], Dll4, Jag1 [Jagged canonical Notch ligand 1], and Jag2) (*B*) mRNAs in lung homogenates from Bleo-treated C57BL/6N mice (Day 7 [d7], d14, and d21) compared with saline-treated control animals (*n* = 4 animals per

various concentrations of Cre and NICD1 (nEGFP) after 2 and 4 weeks of Dox treatment. Thus, only mice with robust expression of both Cre and NICD1 (nEGFP) transgene (*see* Figure E9A, asterisk) were used for further analysis. These mice also displayed increased Hes1 expression in AEC2s in a Dox-dependent manner (*see* Figure E9B).

Histological assessment of NICD1 mice killed after 2 and 4 weeks of Dox treatment revealed an obvious fibrotic phenotype: patchy subpleural or hilar histological appearance of septal thickening, intraalveolar infiltrates, and increased matrix deposition (Figure 6A). In fibrotic areas of Dox-treated NICD1 transgenic mice, the septal thickness and the alveolar mean linear intercept were increased compared with untreated control animals (Figure 6B). Further immunofluorescence staining revealed increased collagen and vimentin expression as well as Ki67 staining in these fibrotic areas of Dox-treated NICD1 mice (Figure 6C). In lung homogenates, extracellular matrix and proliferation markers were significantly increased after 2 (collagen 1, α SMA [α -smooth muscle actin]) and 4 (vimentin, PCNA [proliferating cell nuclear antigen]) weeks of Dox treatment (Figure 6D).

NOTCH Activation Causes Altered SP Processing

In Dox-treated NICD1 transgenic mice, we observed the very same pattern of surfactant abnormalities as in IPF: reduced mSP-B concentrations and accumulation of proSP-B forms (Figure 6F), resulting in a significant decrease in the ratio of mSP-B to total SP-B (*see* Figure E9C). Immunofluorescence

analysis revealed the absence of mSP-B in fibrotic areas but normal expression in nonfibrotic areas of Dox-treated NICD1 mice (Figure 6E). To activate Notch signaling in human AEC2s isolated from donor lungs, these were treated for 16 hours with recombinant DLL1, which caused a marked loss of Napsin A activity (Figure 6G), suggesting a direct involvement of Notch signaling in SP processing.

Inhibition of Notch Signaling Restores AEC2 Differentiation and Reverses Lung Fibrosis

To better understand if blocking Notch signaling could prevent defective surfactant processing in AEC2s, we followed an ex vivo and in vitro approach using MLE12 cells and human PCLSs. MLE12 cells treated with the Notch inhibitor DAPT showed a dose-dependent, significant increase in LysoTracker fluorescence intensity, a surrogate of the epithelial surfactant compartment (32), and reduced Hes1 and NICD1 protein concentrations compared with vehicle control (see Figures E10A-E10C). After determining the optimum DAPT concentration (50 µM; see Figure E10D), human IPF PCLSs were treated for 4 days with 50 µM DAPT versus DMSO. DAPTtreated IPF PCLSs showed 1) a decrease in Hes1 expression (Figure 7A); 2) an increase in LysoTracker uptake (Figure 7B); 3) an increase in mean fluorescence intensity (Figure 7C; see Figure E10E), but not in the number (see Figure E10F) of LysoTracker^{pos} cells in fluorescence-activated cell sortersorted epithelia (EPCAM^{pos} CD45^{neg} CD31^{neg} live); 4) an increase in Napsin A (Figure 7D) protein expression; 5) more prominent staining for mSP-B (but not SP-C; Figure 7E;

see Figure E10H); and 6) an increase in the number of HTII-280 and mSP-B dual-positive cells as assessed by fluorescence-activated cell sorter (Figure 7F; see Figure E10G). Finally, treatment of human IPF PCLSs with DAPT also resulted in a remarkable loss of trichrome staining (see Figure E10I) and collagen 1 expression (Figure 7G) compared with DMSO treatment alone.

DAPT- versus DMSO-treated human IPF PCLSs were also subjected to peptidebased kinase activity profiling of serine/ threonine and tyrosine kinases (Figures 7H and 7I; see Figure E11). DAPT treatment resulted in an overall increase in the activity of most kinases. We identified 23 DAPTresponsive kinases (bar graph illustration in Figure 7H; see overview in Figure E11) including Jak1 and Jak2. Interestingly, these two are key members of the Jak-STAT signaling pathway that we identified to be likewise differentially regulated in IPF septa (Figure 4A; see Table E4). Moreover, pathway analysis of predicted substrates of Notch-modulated kinases demonstrated a statistically significant impact on cell cycle genes and pathways that are of crucial importance for AEC2 identity and function: Wnt, MAPK (mitogen-activated protein kinase), IL-6 (Jak-STAT), and TP53 (tumor protein P53) (Figure 7I) (33, 34).

Discussion

Surfactant alterations have been described in IPF (8, 35) and in experimental lung fibrosis (36, 37), but the underlying reasons have remained obscure. Here we show that the pronounced increase in alveolar surface

Figure 5. (Continued). group, n = 2-4 for quantitative PCR analysis according to sample availability). Mean delta cycle threshold (Δ Ct) (Ct_{housekeeping} – Ct_{gene of interest}) values ± SD are given. *P < 0.05 by unpaired Student's t test. Application of a nonparametric test (aligned rank transformation) for data in B produced similar results, with two changes: Notch3 lost significance at d21, and JAG2 reached significance (asterisk) at d14. (C) Western blot analysis and densitometric quantification of NICD1 and Hes1 (Hes family BHLH transcription factor 1) in saline- and Bleo-treated C57BL/6N mice at d7, d14, d21, and d28 (n=4 per group and time point). β-Actin was used as the loading control. (D) Immunofluorescence analysis of Abca3 (in green) and Notch1 or Hes1 (in red) in d14 saline-treated (control, upper panel) or Bleo-treated (lower panel) mice (n = 4). DAPI was used as nuclear counterstain. Scale bars, 20 μm. (E) Quantification of the number of Hes1-expressing (Hes1^{pos}) AEC2s in saline- versus d14 Bleo-treated mice shown in D. (F and G) Densitometric quantification of western blot analysis of mSP-B (F) and mSP-C (G) in the BALF of saline control animals and Bleo-treated mice. (H) Analysis of western blot densitometric quantification showing the amount of processed mSP-B as the ratio of mSP-B to total SP-B in the lung tissue homogenates of saline control animals and Bleotreated mice. β-Actin was used as the loading control. (I) Western blot analysis (left) and densitometric quantification (right) of Napsin A expression in the lung homogenates of saline control animals and Bleo-treated mice. β-Actin was used as the loading control. (J) Quantitative PCR analysis of Napsa gene expression in the lung homogenates of control and Bleo-treated mice. Actb served as the reference gene. The relative changes in transcript amount with treatments are given by $\Delta\Delta Ct$ values and are expressed as mean \pm SD. Data in C and E-I are presented as mean \pm SEM of log-transformed densitometric values. *P<0.05, **P<0.01, and ***P<0.001 by unpaired Student's t test. Abca3 = ATP-binding cassette subfamily A member 3; Actb = actin beta; AEC2 = type II alveolar epithelial cell; BALF = BAL fluid; mSP-B = mature surfactant protein B; NICD1 = Notch intracellular domain 1; n.s. = not significant; SP-B = surfactant protein B.

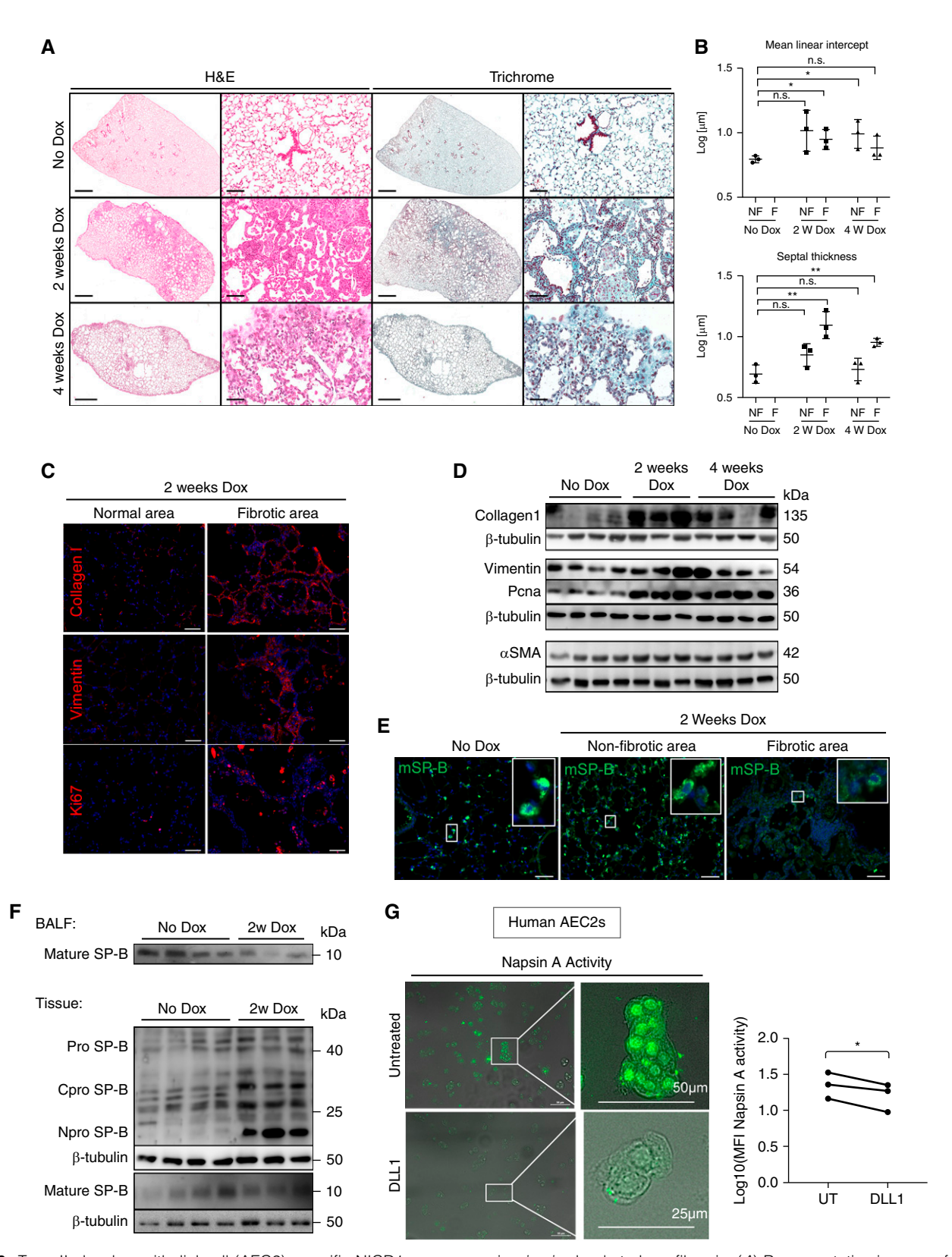


Figure 6. Type II alveolar epithelial cell (AEC2)–specific NICD1 overexpression *in vivo* leads to lung fibrosis. (*A*) Representative images of H&E and Masson's trichrome staining of NICD1 mice untreated (n=3) or doxycycline (Dox) fed for 2 (n=3) or 4 weeks (n=3). Scale bars in low-magnification images, 1 mm; scale bars in high-magnification images, 50 μ m. (*B*) Morphometric analysis of septal thickness and alveolar mean linear intercept of mice as described in *A*. Fibrotic areas (F) and nonfibrotic areas (NF) were analyzed separately. Data are presented as

tension in IPF, and the resulting alveolar collapse during expiration, is caused largely by a massive processing defect of SP-B and -C. Such increase in alveolar surface tension most likely contributes to the loss of pulmonary compliance (as suggested in experimental models of lung fibrosis [38-40]) and to the impaired gas exchange (as evident from V/Q assessment in human IPF [9] and from blood gas analyses in experimental models [10, 39] of lung fibrosis), although we cannot completely rule out a contribution of increased matrix stiffness to alveolar emptying during expiration. It therefore remains an intriguing thought that therapeutic correction of the alveolar surface tension in IPF could help improve lung mechanics, gas exchange, or both, as in infant or acute respiratory distress syndrome (41, 42). Using an opposite approach, experimental inhibition of surfactant processing leading to profound loss of mSP-B in the mouse lung was sufficient to cause overt lung fibrosis. This is reminiscent of the very rare cases of inherited SP-B deficiency with partial defects in SP-B production, in which affected children survive beyond the neonatal period and develop interstitial lung disease (43). Possible explanations for interstitial lung disease development could be enhanced AEC2 injury via ER stress (as shown in here in vitro and in vivo) or via enhanced stretch of AEC2 due to repetitive alveolar collapse (44) or stretch-induced, $\alpha v\beta 5$ integrin-mediated, direct activation of TGF-β in the neighboring mesenchyme (45). Following this concept, it is intriguing to consider the subpleural, basal onset and predominance of reticulation in IPF (26) as a result of one or more of the following processes: 1) a permanent and global elevation in alveolar surface tension,

as shown herein; 2) lower retractive forces of neighboring tissue in the subpleural space; and 3) a higher transpulmonary pressure gradient in the subpleural and basal lung regions.

Importantly, we identified Notch signaling as a major pathway differentially regulated in IPF and demonstrate that Notch1, in particular, is activated in AEC2s of patients with IPF and bleomycin-injured mouse lungs, which is in line with recent single cell-based analyses of IPF epithelia (46, 47). As the Notch signature was evident in (still) normal-appearing septa in human IPF and early after bleomycin treatment (this study), or after Pseudomonas aeruginosa application in a lung injury model (19), it can be postulated that the Notch response occurs early in response to injury and does not represent a late-stage phenomenon.

Notch1 activation in vitro and in vivo also resulted in decreased Napsin A activity and defective SP-B processing, providing a possible explanation for the surfactant defects encountered in subjects with IPF. This was reinforced by the observation that blockade of Notch signaling in IPF PCLS ex vivo was sufficient to augment and restore surfactant storage and processing. Notch signaling plays a major role during lung development (23, 48), and it deeply affects the differentiation of epithelial-specific lineages in the airway epithelium (49–52) and alveolar cell fate decisions (23, 53). Although further work is necessary to decipher the precise mechanism by which Notch regulates AEC2 proliferation and surfactant processing, our study proposes Jak-Stat signaling as an important downstream effector of Notch signaling in the injured alveolar epithelium in IPF.

Jak-Stat is a well-known regulator of surfactant secretion (54), but little is known about its role in surfactant synthesis and processing (34). Hence, loss of differentiation of AEC2 may be the price to be paid for Notch-induced proliferation (and regeneration) of this cell pool.

Moreover, AEC2-specific overexpression of NICD1 in the mouse lung resulted in irregular, patchy, and in part subpleural and aberrant collagen deposition, and blocking of Notch signaling in human IPF PCLS resulted in a clear reduction in collagen deposition. However, lung fibrosis was not described in a similar NICD1 overexpression study (53), which may be due to the different degree and spatial localization of NICD1 expression inherent to the transgenic mouse models used. We therefore believe that there is a threshold degree and spatial distribution of Notch activation beyond which lung fibrosis, either via the aforementioned disturbances in the surfactant system or by paracrine activation of mesenchymal cells, develops. In this line of reasoning, it appears desirable to better understand the mutual interaction between the Notch system and the most important meditator of fibrosis, TGF-β. Activation of the TGF-β pathway has been shown in this study in response to NICD1 overexpression (see Table E4), but it is also known that active TGF-β signaling may cause Notch activation (reviewed in Reference 55).

Recent single-cell transcriptomic data in mouse and human lung identified several populations of alveolar epithelial cells with intermediate transcriptomic signatures, suggestive of transitional states between different cell fates (27, 30, 56, 57). In IPF, transitional AEC2s found between AEC2s and AEC1s (56), as well as cells bearing

Figure 6. (*Continued*). mean \pm SEM of log-transformed densitometric values. *P<0.05 and **P<0.01 by unpaired Student's t test. (*C*) Immunofluorescence analysis of collagen I, vimentin, and Ki67 expression in normal (i.e., NF) areas and F areas in NICD1 mice exposed to Dox for 2 weeks. DAPI was used as nuclear counterstain. Scale bar, 50 μm. (*D*) Lung homogenates from mice as in A were subjected to western blot analysis (left) for collagen 1, vimentin, PCNA, and αSMA. β-Tubulin served as the loading control. Data are presented as mean \pm SEM of log-transformed densitometric values. *P<0.05 by unpaired Student's t test. (E) Immunofluorescence staining of mature surfactant protein B (mSP-B; green signal) was performed on lung tissue from mice as in A. DAPI was used as a nuclear counterstain. Scale bar, 50 μm. (F) Western blot analysis of lung tissues and BAL fluid (BALF) from NICD1 transgenic mice unexposed (n=3) or exposed to Dox for 2 weeks (n=3) using antibodies against proSP-B and mSP-B. β-Tubulin served as the loading control. For BALF analysis, equivalent volumes were loaded. Data are presented as mean \pm SEM of log-transformed densitometric values. *P<0.05 by unpaired Student's t test. (G) Napsin activity of fluorescence-activated cell sorter-isolated human AEC2s (n=3) cultured for 12–16 hours in the presence (below) or absence (above) of 3 μg/ml recombinant human DLL1 (Delta like canonical Notch ligand 1). Right graph represents quantification of the mean fluorescence intensity in DLL1- and control-treated cells. Scale bars in untreated control, 50 μm; scale bars in DLL1 treated, 25 μm. Data were paired per patient. *P<0.05 by paired Student's t test. t0 weeks; t0 weeks; t1 when t2 weeks; t3 has a proliferating cell nuclear antigen.

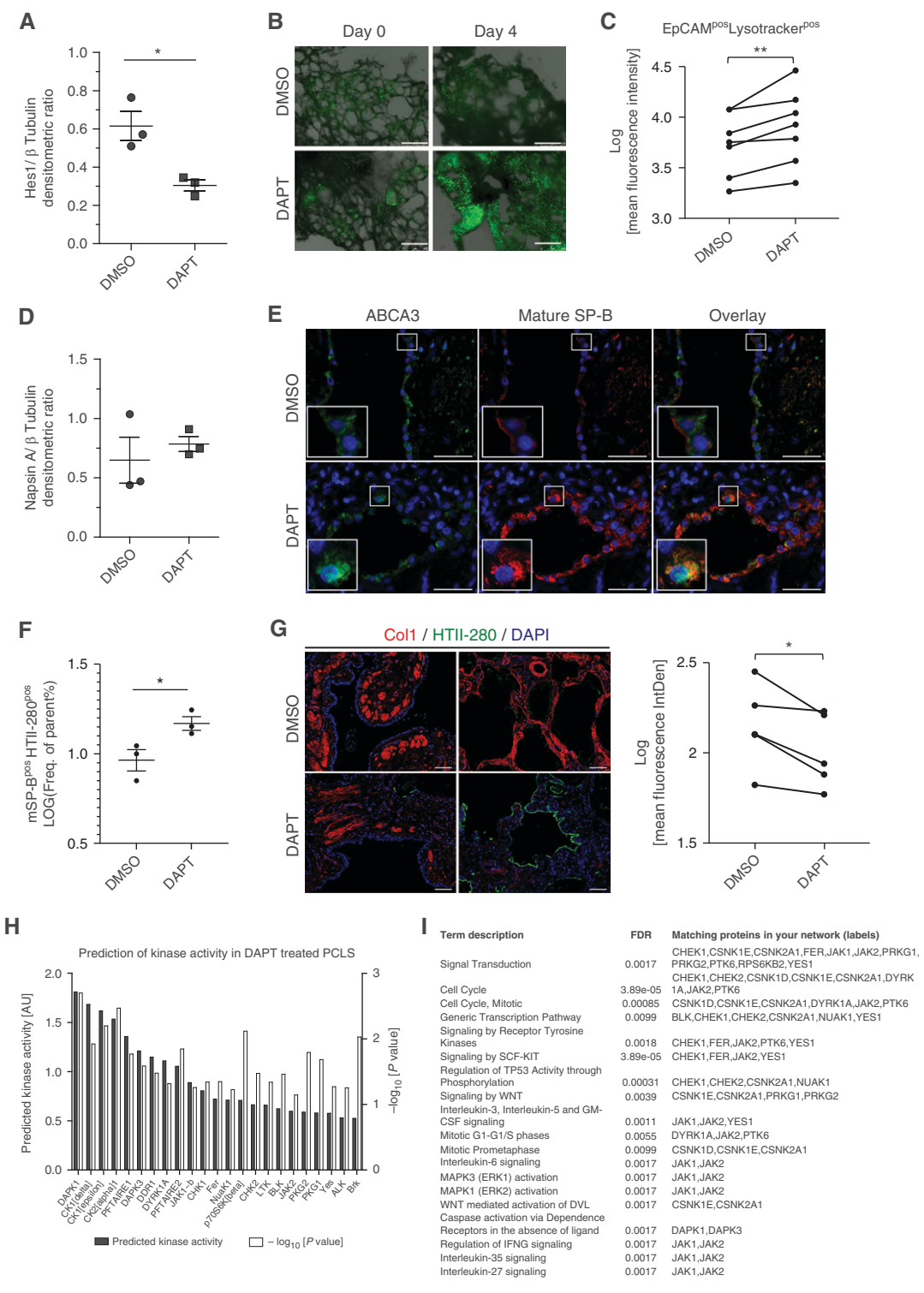


Figure 7. Inactivation of Notch signaling restores type II alveolar epithelial cell (AEC2) differentiation and reverses lung fibrosis. (*A*) Densitometric quantification of Hes1 western blot analysis in three N-[N-(3,5-difluorophenacetyl-L-alanyl)]-S-phenylglycine t-butyl ester (DAPT) (50 μM) versus three DMSO (controls; 4 days) treated precision-cut lung slice (PCLSs) from one patient with idiopathic pulmonary fibrosis (IPF). β-Tubulin served as the loading control. Statistical analysis was performed on \log_{10} densitometric values. *P< 0.05 by unpaired Student's t test. (B) Live fluorescence imaging of human IPF PCLSs cultured in DMSO or DAPT (50 μM) for 4 days in the presence of LysoTracker Green. Representative overlaid phase contrast and LysoTracker Green images (n = 4 patients with IPF) at Day 0 and 4 days are shown. Scale bars, 500 μm. (C) Flow cytometry analysis of LysoTracker incorporation in the DAPI^{neg}, CD45^{neg}, CD31^{neg}, EpCAM (epithelial cell adhesion molecule)^{pos} population of IPF PCLSs (three PCLSs per condition per patient, n = 7 patients) cultured for 4 days in the presence of DMSO or DAPT. Graph shows

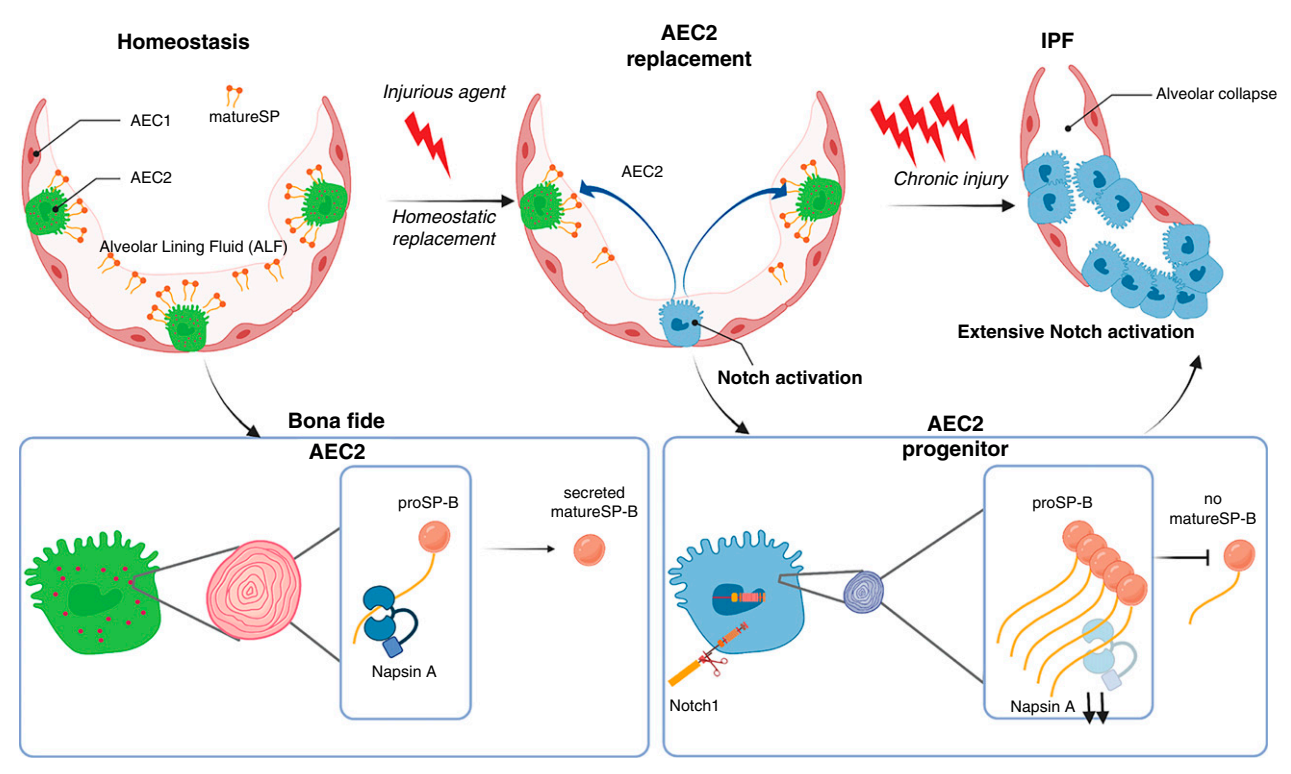


Figure 8. Summary of the data. In homeostatic conditions, type II alveolar epithelial cells (AEC2s) process and secrete SP (surfactant protein), which is responsible for maintaining low BAL fluid surface tension, allowing optimal alveolar function during the respiratory cycle. To replace damaged or aging AEC2s, rare AEC2s downregulate their surfactant-related function through activation of Notch signaling, allowing them to exert their progenitor function. However, in IPF, vicious cycles of alveolar epithelial injury and repair, governed by widespread Notch activation, lead to a generalized decrease in mature SP, increased alveolar surface tension and collapse, and stretch-induced additional alveolar injury. For details see Discussion. AEC1 = type I alveolar epithelial cell; BALF = BAL fluid; IPF = idiopathic pulmonary fibrosis.

Figure 7. (Continued), quantification of log₁₀(mean fluorescence intensity) of DAPI^{neg}, CD45^{neg}, CD31^{neg}, EpCAM^{pos}, LysoTracker Green^{pos} cells. **P < 0.01 by paired Student's t test. (D) Densitometric quantification of Napsin A western blot analysis in three DAPT (50 μM) versus three DMSO (controls; 4 days) treated PCLSs from one patient with IPF. β-Tubulin served as the loading control. Statistical analysis was performed on log₁₀ densitometric values. (E) Immunofluorescence staining with an antibody specific for mature surfactant protein B (mSP-B; red) in DAPT- versus DMSO-treated human IPF PCLSs (three PCLS from four patients); shown is a representative image. AEC2s were identified by ABCA3 immunoreactivity (green signal). Scale bars, 20 µm. (F) Flow cytometry analysis of mSP-B intracellular expression in three DAPT (50 μM) versus three DMSO (controls; 4 days) treated PCLSs from one patient with IPF. Graph shows quantification of log₁₀ frequency of parent (%mSP-B^{pos} HTII-280^{pos} of CD45^{neg} CD31^{neg} EpCAM^{pos}). *P<0.05 by unpaired Student's t test. (G) Human IPF PCLSs cultured for 4 days (three PCLS per condition per patient, n=5 patients) in the presence of DMSO or DAPT (50 µM) were analyzed using immunofluorescence staining for collagen 1 (Col1; red) and HTII-280 (green). DAPI was used for nuclear counterstain. Scale bars, 50 µm. Col1 staining intensity is quantified in the adjacent graph. Data are presented as mean ± SEM of log-transformed mean fluorescent intensity. *P<0.05 by paired Student's t test. (H and I) Upstream kinase analysis on the basis of differential peptide phosphorylation of DMSO- and DAPT-treated human PCLS (4 days). (H) Bioinformatically assisted prediction of upstream kinase activity on the basis of the DAPT-specific pattern of substrate peptide phosphorylation yields 23 significantly deregulated kinases for which increased predicted kinase activity (given in arbitrary units) and a specificity score of approximately 1.3 (negative log₁₀[P value] with P=0.05) due to DAPT exposure can be anticipated. (I) Pathway analysis of predicted substrates of Notch-modulated kinases. ABCA3 = ATP-binding cassette subfamily A member 3; ALK = ALK receptor tyrosine kinase; AU = arbitrary units; BLK = BLK proto-oncogene, Src family tyrosine kinase; Brk = protein tyrosine kinase 6; CD = cluster of differentiation; CHEK1 = checkpoint kinase 1; CHK1 = checkpoint kinase 1; CK = casein kinase; CSNK1E = casein kinase 1 epsilon; CSNK2A1 = casein kinase 2 alpha 1 DAPK1 = death associated protein kinase 1; DDR1 = discoidin domain receptor tyrosine kinase 1; DVL = Dishevelled segment polarity protein; DYRK1A = dual specificity tyrosine phosphorylation regulated kinase 1A; FDR = false discovery rate; FER = FER tyrosine kinase; Freq. = frequency; GM-CSF = granulocyte macrophage colony-stimulating factor; Hes1 = Hes family BHLH transcription factor 1; JAK = Janus kinase; KIT = KIT proto-oncogene, receptor tyrosine kinase; LTK = leukocyte receptor tyrosine kinase; MAPK = mitogen-activated protein kinase; NuaK1 = NUAK family kinase 1; p70S6Kbeta = ribosomal protein S6 kinase beta; PFTAIRE1 = cyclin dependent kinase 14; PFTAIRE2 = cyclin dependent kinase 15; PKG2 = protein kinase G2; PRKG1 = protein kinase CGMP-dependent 1; PTK6 = protein tyrosine kinase 6; RPS6KB2 = ribosomal protein S6 kinase B2; SCF = stem cell factor; TP53 = tumor protein P53; YES1 = YES Proto-oncogene 1, Src family tyrosine kinase.

combined basal and AEC2 signatures, have been shown to be expanded (27). Our group recently showed that such intermediate AEC2s are characterized by underrepresented surfactant processing compartment, as identified by LysoTracker incorporation (28). The data presented here suggest that Notch signaling might play an important role in regulating these transitional states. Supporting this idea, Finn and colleagues demonstrated that Notch signaling is activated in AEC2s during the early phase of repair after P. aeruginosainduced injury, but its downregulation is necessary to allow full differentiation toward AEC1s (19). Interestingly, reanalysis and cross-species integration of scRNA data also

identified Notch signaling as a regulator of AEC2s to KRT5 (keratin 5)—/KRT17+ intermediates (58). However, further single-cell transcriptomic analysis in human PCLS in low- or high-Notch conditions is necessary to firmly establish Notch as a regulator of AEC2 transition and understand its precise role in the heterogeneity of this population.

Conclusions

We propose a model in which Notch1 regulates the balance between the proliferative and differentiated functions of AEC2s in the human lung (Figure 8): temporally and spatially limited injury to the alveolar compartment may result in transient

Notch1 activation and dedifferentiation of AEC2s, hence allowing the activation and proliferation of their progenitors and replacement of the alveolar epithelium. Persistent and global alveolar injury, as observed in IPF, however, will result in massive proliferation and dedifferentiation of AEC2s by Notch1 activation, with severe consequences on the surfactant system and alveolar homeostasis and induction of a vicious cycle of increased alveolar surface tension, recurrent alveolar epithelial injury, and repair leading to lung fibrosis.

<u>Author disclosures</u> are available with the text of this article at www.atsjournals.org.

References

- Raghu G, Collard HR, Egan JJ, Martinez FJ, Behr J, Brown KK, et al.; ATS/ERS/JRS/ALAT Committee on Idiopathic Pulmonary Fibrosis. An official ATS/ERS/JRS/ALAT statement: idiopathic pulmonary fibrosis: evidence-based guidelines for diagnosis and management. Am J Respir Crit Care Med 2011;183:788–824.
- Garcia CK. Insights from human genetic studies of lung and organ fibrosis. *J Clin Invest* 2018;128:36–44.
- 3. Katzen J, Beers MF. Contributions of alveolar epithelial cell quality control to pulmonary fibrosis. *J Clin Invest* 2020;130:5088–5099.
- Weaver TE, Conkright JJ. Function of surfactant proteins B and C. Annu Rev Physiol 2001;63:555–578.
- 5. Whitsett JA, Weaver TE. Hydrophobic surfactant proteins in lung function and disease. *N Engl J Med* 2002;347:2141–2148.
- Thomas AQ, Lane K, Phillips J III, Prince M, Markin C, Speer M, et al. Heterozygosity for a surfactant protein C gene mutation associated with usual interstitial pneumonitis and cellular nonspecific interstitial pneumonitis in one kindred. Am J Respir Crit Care Med 2002;165: 1220, 1228.
- 7. Whitsett JA, Wert SE, Weaver TE. Diseases of pulmonary surfactant homeostasis. *Annu Rev Pathol* 2015;10:371–393.
- Günther A, Schmidt R, Nix F, Yabut-Perez M, Guth C, Rosseau S, et al. Surfactant abnormalities in idiopathic pulmonary fibrosis, hypersensitivity pneumonitis and sarcoidosis. Eur Respir J 1999;14:565–573.
- Günther A, Enke B, Markart P, Hammerl P, Morr H, Behr J, et al. Safety and tolerability of bosentan in idiopathic pulmonary fibrosis: an open label study. Eur Respir J 2007;29:713–719.
- Ruppert C, Kuchenbuch T, Boensch M, Schmidt S, Mathes U, Hillebrand V, et al. Dry powder aerosolization of a recombinant surfactant protein-Cbased surfactant for inhalative treatment of the acutely inflamed lung. Crit Care Med 2010;38:1584–1591.
- Korfei M, Ruppert C, Mahavadi P, Henneke I, Markart P, Koch M, et al. Epithelial endoplasmic reticulum stress and apoptosis in sporadic idiopathic pulmonary fibrosis. Am J Respir Crit Care Med 2008;178: 838–846.
- Barkauskas CE, Cronce MJ, Rackley CR, Bowie EJ, Keene DR, Stripp BR, et al. Type 2 alveolar cells are stem cells in adult lung. J Clin Invest 2013; 123:3025–3036.
- Desai TJ, Brownfield DG, Krasnow MA. Alveolar progenitor and stem cells in lung development, renewal and cancer. *Nature* 2014;507: 100–104
- Zacharias WJ, Frank DB, Zepp JA, Morley MP, Alkhaleel FA, Kong J, et al. Regeneration of the lung alveolus by an evolutionarily conserved epithelial progenitor. *Nature* 2018;555:251–255.
- Bolaños AL, Milla CM, Lira JC, Ramírez R, Checa M, Barrera L, et al. Role of Sonic Hedgehog in idiopathic pulmonary fibrosis. Am J Physiol Lung Cell Mol Physiol 2012;303:L978–L990.

- Jenkins RG, Su X, Su G, Scotton CJ, Camerer E, Laurent GJ, et al. Ligation of protease-activated receptor 1 enhances alpha(v)beta6 integrin-dependent TGF-beta activation and promotes acute lung injury. J Clin Invest 2006;116:1606–1614.
- Königshoff M, Kramer M, Balsara N, Wilhelm J, Amarie OV, Jahn A, et al. WNT1-inducible signaling protein-1 mediates pulmonary fibrosis in mice and is upregulated in humans with idiopathic pulmonary fibrosis. J Clin Invest 2009;119:772–787.
- Vaughan AE, Brumwell AN, Xi Y, Gotts JE, Brownfield DG, Treutlein B, et al. Lineage-negative progenitors mobilize to regenerate lung epithelium after major injury. Nature 2015;517:621–625.
- Finn J, Sottoriva K, Pajcini KV, Kitajewski JK, Chen C, Zhang W, et al. Dlk1-mediated temporal regulation of notch signaling is required for differentiation of alveolar type II to type I cells during repair. Cell Rep 2019;26:2942–2954.e5.
- Hori K, Sen A, Artavanis-Tsakonas S. Notch signaling at a glance. J Cell Sci 2013;126:2135–2140.
- Ito T, Udaka N, Yazawa T, Okudela K, Hayashi H, Sudo T, et al. Basic helix-loop-helix transcription factors regulate the neuroendocrine differentiation of fetal mouse pulmonary epithelium. *Development* 2000; 127:3913–3921
- Lafkas D, Shelton A, Chiu C, de Leon Boenig G, Chen Y, Stawicki SS, et al. Therapeutic antibodies reveal Notch control of transdifferentiation in the adult lung. Nature 2015;528:127–131.
- Guseh JS, Bores SA, Stanger BZ, Zhou Q, Anderson WJ, Melton DA, et al. Notch signaling promotes airway mucous metaplasia and inhibits alveolar development. *Development* 2009;136:1751–1759.
- Karmrodt J, Bletz C, Yuan S, David M, Heussel C-P, Markstaller K. Quantification of atelectatic lung volumes in two different porcine models of ARDS. *Br J Anaesth* 2006;97:883–895.
- Mai C, Verleden SE, McDonough JE, Willems S, De Wever W, Coolen J, et al. Thin-section CT features of idiopathic pulmonary fibrosis correlated with micro-CT and histologic analysis. Radiology 2017;283: 252–263.
- Yilmaz C, Watharkar SS, Diaz de Leon A, Garcia CK, Patel NC, Jordan KG, et al. Quantification of regional interstitial lung disease from CT-derived fractional tissue volume: a lung tissue research consortium study. Acad Radiol 2011;18:1014–1023.
- Adams TS, Schupp JC, Poli S, Ayaub EA, Neumark N, Ahangari F, et al. Single-cell RNA-seq reveals ectopic and aberrant lungresident cell populations in idiopathic pulmonary fibrosis. Sci Adv 2020:6:eaba1983.
- Wasnick RM, Shalashova I, Wilhelm J, Khadim A, Schmidt N, Hackstein H, et al. Differential LysoTracker uptake defines two populations of distal epithelial cells in idiopathic pulmonary fibrosis. Cells 2022;11:235.
- Van der Velden JL, Bertoncello I, McQualter JL. LysoTracker is a marker of differentiated alveolar type II cells. Respir Res 2013;14:123.

ORIGINAL ARTICLE

- Strunz M, Simon LM, Ansari M, Kathiriya JJ, Angelidis I, Mayr CH, et al. Alveolar regeneration through a Krt8+ transitional stem cell state that persists in human lung fibrosis. Nat Commun 2020;11:3559.
- Murtaugh LC, Stanger BZ, Kwan KM, Melton DA. Notch signaling controls multiple steps of pancreatic differentiation. *Proc Natl Acad Sci* U S A 2003;100:14920–14925.
- Haller T, Ortmayr J, Friedrich F, Völkl H, Dietl P. Dynamics of surfactant release in alveolar type II cells. *Proc Natl Acad Sci U S A* 1998;95: 1579–1584.
- Park S-K, Dahmer MK, Quasney MW. MAPK and JAK-STAT signaling pathways are involved in the oxidative stress-induced decrease in expression of surfactant protein genes. *Cell Physiol Biochem* 2012;30: 334–346.
- 34. Ladenburger A, Seehase M, Kramer BW, Thomas W, Wirbelauer J, Speer CP, et al. Glucocorticoids potentiate IL-6-induced SP-B expression in H441 cells by enhancing the JAK-STAT signaling pathway. Am J Physiol Lung Cell Mol Physiol 2010;299:L578–L584.
- Schmidt R, Meier U, Markart P, Grimminger F, Velcovsky HG, Morr H, et al. Altered fatty acid composition of lung surfactant phospholipids in interstitial lung disease. Am J Physiol Lung Cell Mol Physiol 2002;283: L1079–L1085.
- Carter CL, Jones JW, Farese AM, MacVittie TJ, Kane MA. Lipidomic dysregulation within the lung parenchyma following whole-thorax lung irradiation: markers of injury, inflammation and fibrosis detected by MALDI-MSI. Sci Rep 2017;7:10343.
- Schmidt R, Ruppert C, Markart P, Lübke N, Ermert L, Weissmann N, et al. Changes in pulmonary surfactant function and composition in bleomycin-induced pneumonitis and fibrosis. *Toxicol Appl Pharmacol* 2004:195:218–231.
- Thrall RS, Swendsen CL, Shannon TH, Kennedy CA, Frederick DS, Grunze MF, et al. Correlation of changes in pulmonary surfactant phospholipids with compliance in bleomycin-induced pulmonary fibrosis in the rat. Am Rev Respir Dis 1987;136:113–118.
- Steffen L, Ruppert C, Hoymann H-G, Funke M, Ebener S, Kloth C, et al. Surfactant replacement therapy reduces acute lung injury and collapse induration-related lung remodeling in the bleomycin model. Am J Physiol Lung Cell Mol Physiol 2017;313:L313–L327.
- Horiuchi T, Mason RJ, Kuroki Y, Cherniack RM. Surface and tissue forces, surfactant protein A, and the phospholipid components of pulmonary surfactant in bleomycin-induced pulmonary fibrosis in the rat. Am Rev Respir Dis 1990;141:1006–1013.
- Niemarkt HJ, Hütten MC, Kramer BW. Surfactant for respiratory distress syndrome: new ideas on a familiar drug with innovative applications. Neonatology 2017;111:408–414.
- Spragg RG, Lewis JF, Walmrath H-D, Johannigman J, Bellingan G, Laterre P-F, et al. Effect of recombinant surfactant protein C-based surfactant on the acute respiratory distress syndrome. N Engl J Med 2004;351:884–892.

- Wert SE, Whitsett JA, Nogee LM. Genetic disorders of surfactant dysfunction. Pediatr Dev Pathol 2009;12:253–274.
- Hammerschmidt S, Kuhn H, Gessner C, Seyfarth H-J, Wirtz H. Stretchinduced alveolar type II cell apoptosis: role of endogenous bradykinin and PI3K-Akt signaling. Am J Respir Cell Mol Biol 2007;37:699–705.
- Wipff P-J, Rifkin DB, Meister J-J, Hinz B. Myofibroblast contraction activates latent TGF-beta1 from the extracellular matrix. *J Cell Biol* 2007;179:1311–1323.
- 46. Xu Y, Mizuno T, Sridharan A, Du Y, Guo M, Tang J, et al. Single-cell RNA sequencing identifies diverse roles of epithelial cells in idiopathic pulmonary fibrosis. JCI Insight 2016;1:e90558.
- Xi Y, Kim T, Brumwell AN, Driver IH, Wei Y, Tan V, et al. Local lung hypoxia determines epithelial fate decisions during alveolar regeneration. Nat Cell Biol 2017;19:904–914.
- Xu K, Moghal N, Egan SE. Notch signaling in lung development and disease. Adv Exp Med Biol 2012;727:89–98.
- Morimoto M, Nishinakamura R, Saga Y, Kopan R. Different assemblies of Notch receptors coordinate the distribution of the major bronchial Clara, ciliated and neuroendocrine cells. *Development* 2012;139:4365–4373.
- Pardo-Saganta A, Law BM, Tata PR, Villoria J, Saez B, Mou H, et al. Injury induces direct lineage segregation of functionally distinct airway basal stem/progenitor cell subpopulations. Cell Stem Cell 2015;16:184–197.
- Tsao P-N, Vasconcelos M, Izvolsky KI, Qian J, Lu J, Cardoso WV. Notch signaling controls the balance of ciliated and secretory cell fates in developing airways. *Development* 2009;136:2297–2307.
- Xing Y, Li A, Borok Z, Li C, Minoo P. NOTCH1 is required for regeneration of Clara cells during repair of airway injury. Stem Cells 2012;30:946–955.
- Allen TD, Rodriguez EM, Jones KD, Bishop JM. Activated Notch1 induces lung adenomas in mice and cooperates with Myc in the generation of lung adenocarcinoma. *Cancer Res* 2011;71:6010–6018.
- Matsuzaki Y, Besnard V, Clark JC, Xu Y, Wert SE, Ikegami M, et al. STAT3 regulates ABCA3 expression and influences lamellar body formation in alveolar type II cells. Am J Respir Cell Mol Biol 2008;38: 551–558.
- Zhang Y, Jin D, Kang X, Zhou R, Sun Y, Lian F, et al. Signaling pathways involved in diabetic renal fibrosis. Front Cell Dev Biol 2021;9:696542.
- 56. Jiang P, Gil de Rubio R, Hrycaj SM, Gurczynski SJ, Riemondy KA, Moore BB, et al. Ineffectual type 2-to-type 1 alveolar epithelial cell differentiation in idiopathic pulmonary fibrosis: persistence of the KRT8^{hi} transitional state. Am J Respir Crit Care Med 2020;201:1443–1447.
- 57. Kobayashi Y, Tata A, Konkimalla A, Katsura H, Lee RF, Ou J, et al. Persistence of a regeneration-associated, transitional alveolar epithelial cell state in pulmonary fibrosis. *Nat Cell Biol* 2020;22:934–946.
- Huang KY, Petretto E. Cross-species integration of single-cell RNAseq resolved alveolar-epithelial transitional states in idiopathic pulmonary fibrosis. Am J Physiol Lung Cell Mol Physiol 2021;321: L491–L506.